Variations in the East Asian summer monsoon over the past millennium and their links to the Tropic Pacific and North Atlantic oceans

Fucai Duan[a,*], Zhenqiu Zhang[b,c,*], Yi Wang[d,e,*], Jianshun Chen[a], Zebo Liao[c], Shitao Chen[c], Qingfeng Shao[c], Kan Zhao[c]

[a]College of Geography and Environmental Sciences, Zhejiang Normal University, Jinhua 321004, China
[b]School of Life Sciences, Nanjing Normal University, Nanjing 210023, China
[c]College of Geography Science, Nanjing Normal University, Nanjing 210023, China
[d]Department of Geography and School of Global Studies, University of Sussex, Falmer, Brighton BN1 9QJ, UK
[e]Department of Earth System Science, Institute for Global Change Studies, Tsinghua University, Beijing 100084, China

*Corresponding authors:
E-mail addresses: fcduan@foxmail.com (F. Duan), zhangzhenqiu163@163.com (Z. Zhang), yi.wang@sussex.ac.uk (Y. Wang)

Abstract: Variations of East Asian summer monsoon (EASM) during the last millennium could help enlighten the monsoonal response to future global warming. Here we present a precisely dated and highly resolved stalagmite $\delta^{18}O$ record from the Yongxing Cave, central China. Our new record, combined with a previously published one from the same cave, indicates that the EASM has changed dramatically in association with the global temperature rising. In particular, our record shows that the EASM has intensified during the Medieval Climate Anomaly (MCA) and the Current Warm Period (CWP) but weakened during the Little Ice Age (LIA). We find that the EASM intensity is similar during the MCA and CWP periods in both northern and central China, but relatively stronger during the CWP in southern China. This discrepancy indicates a complicated regional response of the EASM to the anthropogenic forcing. The intensified and weakened EASM during the MCA and LIA matches well with the warm and cold phases of Northern Hemisphere surface air temperature, respectively. This EASM pattern also corresponds well with the rainfall over the tropical Indo-Pacific warm pool. Surprisingly, our record shows a strong association with the North Atlantic climate as well. The intensified (weakened) EASM correlates well with positive (negative) phases of North Atlantic Oscillation. In addition, our record links well with the strong (weak) Atlantic meridional overturning circulation during the MCA (LIA) period. All above-mentioned correlations indicate that the EASM tightly couples with oceanic processes in the tropical Pacific and North Atlantic oceans during the MCA and LIA.

Keywords: Stalagmite; East Asian summer monsoon; Global warming; Last

Millennium; Little Ice Age; Medieval Climate Anomaly

1 Introduction

The last millennium was climatically characterized by the Medieval Climate Anomaly (MCA; 900-1400 AD) and the Little Ice Age (LIA; 1400-1850 AD), and the Current Warm Period (CWP; 1850AD to present). These three episodes attract broad attention within the scientific and policy-making communities, because they contain critical information to distinguish between the natural and anthropogenic climate variability. Origins of the MCA and LIA are attributed to the radiative forcing associated with solar activities and volcanic eruptions, yet the CWP is considered as a result of increasing anthropogenic greenhouse gases. In particular, the CWP is much warmer than the MCA (Man et al., 2009; Chen et al., 2018). In association with the global temperature change, East Asian summer monsoon (EASM) precipitation has changed significantly. Many studies have indicated that monsoonal climate of China has generally recorded wetter MCA and drier LIA in the north but reverse conditions in the south (Tan et al., 2009; Chen et al., 2015; Xu et al., 2016; Tan et al., 2018). However, it is unclear about the variation of EASM during the MCA and LIA over central China. Moreover, less is known about the relative intensity of EASM between the CWP and MCA, two recent warm periods. The examination of the relative monsoon intensity is the key to evaluating the monsoon response to the anthropogenic warming.

To better understand monsoonal responses to the global warming climatic condition, it is necessary to appreciate the natural forcing of EASM during the MCA and LIA periods. The EASM is strongly influenced by the Tropical Pacific and North Atlantic Oceans. The Pacific Ocean feeds the warm and moisture air directly into the EASM, and therefore exerts a strong influence. Several studies have indicated that the mean-state of EASM is affected by alternations of La Nina-like and El Nino-like conditions in the Tropical Pacific during the last millennium (Cobb et al., 2003; Yan et al., 2011a; Rustic et al., 2015; Chen et al., 2018). However, these studies did not reach an agreement on how the Tropical Pacific affects EASM. To precisely understand the EASM dynamics, we need to know which changes in EASM are linked to which modes of the Pacific atmosphere-ocean circulation during the MCA and LIA in central China. The North Atlantic signal can be transmitted to other parts of the world through the Atlantic meridional overturning circulation (AMOC; Bond et al., 2001). Marine sedimentary records have suggested that strong (weak) AMOC over the warm Greenland interstadials (stadials) correlated with intervals of enhanced (reduced) EASM during the last glaciation (Wang et al., 2001; Jiang et al., 2016). Similarly, weak EASM episodes occurred in association with ice-rafted events in the North Atlantic, which is capable of weakening the AMOC during the Holocene (Wang et al., 2005; Zhao et al., 2016). This covariation implies a persistent influence of the AMOC on EASM. However, there is no direct evidence to support the link between the AMOC and EASM during the MCA and LIA intervals.

Here we present a new precisely-dated and highly-resolved stalagmite record from Yongxing Cave, Central China. This record, together with a recently published records from the same cave (Zhang et al., 2019), advances our understanding of the EASM dynamics during the last millennium.

2 Materials and methods

Two stalagmites (YX262 and YX275) are used in this study, both are from Yongxing Cave (31°35′N, 111°14′E; elevation 800 m above msl), central China. The previously published stalagmites YX275 has reported detailed variability in the EASM since the LIA (Zhang et al., 2019). The new candle-like stalagmite YX262 is 159 mm long and 55 mm wide. The Yongxing Cave is located between the Chinese Loess Plateau and the Yangtze River. Average annual rainfall is about 1000 mm at the site of the cave. Atmospheric temperature is about 14.3 ℃ and relative humidity is close to 100% inside the cave. The cave site is climatically influenced by East Asian Monsoon, featured with wet and warm summer, and dry and cold winter.

Stalagmite YX262 was first halved and then polished for the purpose of the subsequent sampling. For stable isotope analyses, powdered subsamples, weighing about 50-100 μg, were drilled on the polished surface along the central growth axis of the stalagmite. A total of 159 subsamples were obtained at 1 mm increments. The $\delta^{18}O$ measurements were performed on a Finnigan-MAT-253 mass spectrometer at Nanjing Normal University. Results are reported as per mil (‰) against the standard Vienna Pee Dee Belemnite (VPDB). Precision of $\delta^{18}O$ is 0.06‰ at the 1-sigma level. For U-Th dates, six powdered subsamples, about 100 mg each, were drilled along the central growth layer. Procedures for chemical separation and purification of uranium and thorium were described in Shao et al. (2017). U and Th isotope measurements were performed on a Neptune MC-ICP-MS at Nanjing Normal University. All the dates are in stratigraphic order with uncertainty of less than 0.03% of the actual dates.

3 Results

3.1 Chronology

The six U-Th dates and corresponding isotopic rations are shown in Table 1. Adequate uranium concentrations (0.5–0.7 ppm) and low initial thorium contents (200–700 ppt, with the exception of 1440 ppt) produced precise dates with small age uncertainty (6–20 years). The chronology for the stalagmite was established by the StalAge algorithm (Scholz and Hoffmann, 2011). The age model shows that the stalagmite YX262 was deposited from 1027 to 1639 AD (see Fig. 2). The age-depth plot indicates the growth rate of the stalagmite is stable, reaching 0.26 mm/year. The high and stable growth rate suggests that the stalagmite grew continuously without a significant hiatus. Visual inspections consolidate the continuity of the stalagmite growth. The temporal resolution is 3.8 year, allowing for detailed characterizing the Asian hydroclimate for the first half of the second millennium.

3.2 Stable isotope

The $\delta^{18}O$ record of YX262 displays a pronounced fluctuation during the whole period (see Fig. 3). The $\delta^{18}O$ values ranges from -9.31‰ to -7.88‰, averaging -8.60‰. The $\delta^{18}O$ values decrease gradually from 1027 to 1372 AD, and then increase gradually before rapidly increasing to the ^{18}O-enriched conditions from 1515 AD. The interval with high $\delta^{18}O$ values is ~100-year long, which is terminated by a pulse to more negative values at 1626 AD. In general, the ^{18}O-depleted interval is coeval with the MCA and the ^{18}O-enriched interval corresponds to the early LIA (see Fig. 3).

4 Discussion

4.1 The interpretation of our $\delta^{18}O$

Stalagmite YX262 was deposited under the condition of isotope equilibrium. Relative to the Hendy tests, replication tests have been considered as a more vigorous method to examine the isotope equilibrium (Dorale and Liu, 2009). The YX262 $\delta^{18}O$ record matches another Yongxing cave record during the overlapping interval (see Fig.

4; Zhang et al., 2019), indicating an equilibrium condition for the isotope. Thus, the YX262 $\delta^{18}O$ signal is less influenced by the kinetic fractionation and is primarily of climatic origin. Nevertheless, the climatic significance of the cave $\delta^{18}O$ record in eastern China remains a long-term scientific debate. The cave $\delta^{18}O$ records are normally interpreted as large-scale and integrated changes in the Asian summer monsoon intensity (e.g., Wang et al., 2001; 2005; Cheng et al., 2009; 2016). This interpretation is supported by strong correlations among the cave $\delta^{18}O$ records across China (e.g., Yuan et al., 2004; Zhao et al., 2010; Li et al., 2014), and by covariations of the $\delta^{18}O$ records with other proxy records reflecting the monsoon intensity or local rainfall (e.g., Goldsmith et al., 2017; Zhao et al., 2015; Owen et al., 2016). However, some studies have revealed that the calcite $\delta^{18}O$ records reflect changes in moisture sources (e.g., Pausata et al., 2011), in particular, regarding the lower (higher) $\delta^{18}O$ values derived from Indian Ocean-dominated (Pacific Ocean-dominated) moisture sources (e.g., Maher and Thompson, 2012; Tan, 2014). Two most recent studies have reconciled these two contradictory interpretations (Orland et al., 2015; Wang et al., 2018). They found that the Chinese stalagmite $\delta^{18}O$ records documented a combination of changes in the isotopic fractionation of water vapor sourced from the Indian and/or Pacific Oceans, and changes in summer monsoon intensity. In reality, the extent of the isotopic fractionation of water vapor from the tropical oceans reflects the changes in integrated monsoon rainfall between the tropical oceans and cave sites (Yuan et al., 2004). Thus, the stalagmite $\delta^{18}O$ signal reflects the regional summer monsoon intensity (Orland et al., 2015; Tan et al., 2015), with lower $\delta^{18}O$ values reflecting stronger monsoon and higher $\delta^{18}O$ values weaker monsoon (Cheng et al., 2016).

4.2 The regional characters of the MCA and LIA

The climate condition during the MCA and LIA has been extensively studied for the monsoonal China (e.g., Chen et al., 2015; Xu et al., 2016; Tan et al., 2018). In general, wetter in the north and drier in the south were inferred during the MCA and the opposite during the LIA (Chen et al., 2015; Tan et al., 2018). The boundary between the north and south of China was estimated to be about along the River Huai at 34°N (Chen et al., 2015), the modern geographical dividing line between northern and southern China. As an interesting exception, the Dongge cave records in Guizhou, Southwestern China (25°17′N, 108°5′E) showed a wetter MCA and drier LIA (see Fig.

3; Wang et al., 2005; Zhao et al., 2015). This is consistent with strong spatiotemporal variability of precipitation in the broad EASM region. Here our Yongxing record, slightly south to 34 °N, shows a similar condition as the Dongge Cave (see Fig. 3). As illustrated in Fig. 3, the stalagmite records from the two caves show a general similarity in shape and thus each of them truthfully registers the broad climate signal. An extra comparison shows that the Yongxing and Dongge records in the south vary broadly in agreement with the Wanxiang (Zhang et al., 2008) and Huangye (Tan et al., 2011) records in the north, indicating the wetter MCA and drier LIA (see Fig. 3). However, a minor but important discrepancy exists between the northern and southern cave records during the MCA. The cave records in the south display an increasing monsoon trend, but those in the north reflect a decreasing monsoon trend during the MCA (see Fig. 3 for trends indicated by the arrows). To explain this discrepancy, we compare all our cave records to changes in temperatures of Northern Hemisphere (Mann et al., 2009) and northern China (Tan et al., 2003), and meridional displacement of the Intertropical Convergence Zone (ITCZ; Haug et al., 2001). The result indicates that the cave records in the south and north collectively exhibit a broad similarity to the variation in the temperatures and the displacement of the ITCZ (see Fig. 3). Detailed inspection displays that the weakening monsoon signal recorded in the northern caves of China during the MCA parallels with the decreasing temperatures in the Northern Hemisphere and northern China. In contrast, the intensified monsoon signal recorded in the southern caves of China during the MCA corresponds to the northward displacement of the ITCZ. The comparison indicates that the different climate patterns between the south and north may result from different controlling factors at lower and higher latitudes, respectively. It seems that the cold temperature from the north restrains the northward migration of the monsoonal rain belt related to the movement of the ITCZ during the MCA, leading to the hydrological seesaw between the north and south. It is noted that the enhanced monsoon condition documented in the Yongxing and Dongge records is contradictory with those reported in many other paleoclimate records in the south. For example, drier MCA and wetter LIA were suggested in an integrated stalagmite $\delta^{18}O$ record from Sichuan Province (Tan et al., 2018), a pollen-derived rainfall record near the Yongxing Cave site (He et al., 2003), and a lake-based rainfall record in Guangdong Province (Chu et al., 2002). This regional discrepancy can be checked by additional highly-resolved and precisely dated records in southern China.

4.3 The monsoon intensity during the MCA as compared to the CWP

A comparison of the relative intensity of EASM between the MCA and CWP could be useful to evaluate the response of EASM towards the current global warming. Many studies have found that the CWP is much warmer than the MCA on global and hemispheric scales (Bradley et al., 2003; Mann et al., 2008, 2009; PAGES 2k Consortium, 2013). With regard to the hydrological response, northern China shows a stronger or comparable monsoon condition during the MCA as compared to the CWP (e.g., the Wangxiang and Huangye Caves' records in Fig. 3). A similar monsoon condition is also documented in the Yongxing record in central China (see Fig. 4). However, two Dongge records in southern China collectively shows a slightly weaker monsoon condition during the MCA as compared to the CWP (see Figs. 3, 4). This is indicated by an overall 0.39‰ higher $\delta^{18}O$ value during the MCA than the CWP (Fig. 4). The stronger monsoon condition during the CWP relative to the MCA is parallel to the global temperature evolution, in particular in the western Pacific Warm Pool region (Chen et al., 2018). This correspondence supports the hypothesis that current global warming intensifies the Asian summer monsoon (Wang et al., 2013). The intensified Asian summer monsoon was suggested due to strong coupling of the climate system related to the global warming. Wang et al. (2013) have stated a mega ENSO condition could trigger a stronger EASM in the CWP through the intensified Hadley and Walker circulations. On the other hand, southern China is partially influenced by the Indian Ocean, which also brings moisture to the area of our study (An et al., 2011). We suggest the small discrepancy between Yongxing and Dongge records could be due to the different localized effects in southern China as Dongge Cave is much closer to Indian Ocean than Yongxing Cave.

Different scenarios exist in the South China Sea regarding to the hydrologic variation between the MCA and CWP. The South China Sea is climatically influenced by the EASM and tropical Pacific climate. The lacustrine and coralline records collectively indicate a comparative climate condition between the MCA and CWP (Yan et al., 2011b; Deng et al., 2017). The MCA and CWP are considered to be drier than the LIA in the South China Sea. Yan et al. (2011b) highlighted that a decrease and eastward shift of the Pacific Walker circulation were responsible primarily for the drier climate condition during the MCA and CWP. However, changes in the Walker circulation (Yan et al., 2011b) are in contrast to other estimations (Wang et al., 2013; Cobb et al., 2003), which suggested a strong Pacific Walker circulation during the warm periods. Due to the contradiction on the Pacific Walker circulation changes, the trigger for the intensified Asian monsoon during the CWP needs further verification. Therefore, continued studies are needed on the links between the EASM and the Pacific climate.

4.4 The link to the Tropical Pacific Ocean

The ITCZ and El Niño-Southern Oscillation (ENSO) exert profound influences on the precipitation in East Asia during the last millennium (Wang et al., 2013). As shown in Fig. 5, our calcite record shows a great similarity to temperature and hydrology reconstructions over the tropical Indo-Pacific warm pool (IPWP). High-resolution sediment (Oppo et al., 2009) and speleothem (Griffiths et al., 2016) records over the IPWP collectively suggest warm sea surface temperatures and reduced rainfall during the MCA and CWP, and reversed conditions during the LIA (Fig. 5). The rainfall over the IPWP is anti-phased with the EASM intensity, supporting the modulation of the ITCZ' latitudinal migration on the EASM during the last millennium (Zhao et al., 2015; Xu et al., 2016; Griffiths et al., 2016). In addition, the temperature change over the IPWP can influence the EASM intensity via the expansion and contraction of the ITCZ (Yan et al., 2015; Chen et al., 2018). The warm MCA and cold LIA conditions do not necessarily signify a La Nina-like condition during the MCA and an El Nino-like condition during the LIA over the IPWP. Conversely, rainfall-based ENSO reconstructions showed the El Nino- and La Nina-like conditions during the MCA and LIA, respectively (Moy et al., 2002, Yan et al., 2011a; Fig. 5e, f). The sediment-derived ENSO variation in Ecuador (Moy et al., 2002) and the composite ENSO reconstruction across the Tropic Pacific (Yan et al., 2011a) showed a great similarity among the ENSO signals and the timing of switches between the ENSO cold and warm phases. These ENSO reconstructions resemble well with Yongxing records (Fig. 5). For example, the El Nino- and La Nina-like conditions during the MCA and LIA parallel with the intensified and weaken EASM from the Yongxing Cave, respectively. In particular, the switch of the ENSO phases from the MCA to LIA coincides with the EASM intensifying peak during the MCA (Fig. 5). These strong correlations indicate a dynamical link between the EASM intensity and ENSO modes. In the summer after the El Niño evolves to maturity, an abnormally blocked anticyclone takes place in Northeast Asia. At the same time, the subtropical high in the western North Pacific extends westward abnormally. This abnormal circulation pattern strengthens the EASM in subtropical East Asia (Wang et al., 2001). Despite the potential monsoon-ENSO link, the ENSO reconstructions still need further verification due to their different variations. A recent temperature record in eastern equatorial Pacific (Rustic et al., 2015) supports the rainfall-based ENSO reconstruction (Moy et al., 2002; Yan et al., 2011a), with the El Nino- and La Nina-like mode during the MCA and LIA, respectively. This record challenges the paradigm of the La Nina-like pattern during the MCA followed by the El Nino-like pattern during the LIA (Cobb et al., 2003). However, the study of Rustic et al. (2015) showed the strongest El Nino-like situation occurred at the late MCA to early LIA transition, instead of the peak MCA.

4.5 The link to the North Atlantic Climate

Surprisingly, our Yongxing record shows a good correlation with the North Atlantic climate. As illustrated in Fig. 6, the intensified (weakened) EASM during the MCA (LIA) coincides with a persistent positive (neutral to slightly negative) North Atlantic Oscillation index (NAO; Trouet et al., 2009; Fig. 6c). In addition, these EASM variations resemble changes of the Atlantic meridional overturning circulation (AMOC), measured by the drift ice index (Bond et al., 2001; Fig. 6d) and mean grain size of sortable silt (Fig. 6e; Thornalley et al., 2018) in the North Atlantic. The intensified EASM corresponds to the strong AMOC during the MCA and the weakened EASM to the weak AMOC during the LIA, which is consistent with the scenario during the last glaciation (Wang et al., 2001; Böhm et al., 2015). These strong correlations indicate an influence of the NAO and AMOC on the EASM. During the MCA, positive NAO induces a warmer winter in Europe, which reduces snow accumulation over Eurasia and therefore allows for a penetration inland of the EASM next summer (Overpeck et al., 1996). Robust AMOC can intensify the EASM through northward positioning the ITCZ (Wang et al., 2017). During the LIA, weaker NAO and AMOC would produce decreased EASM in the reversed fashion. It has been proposed that conditions of the NAO were dynamically coupled to states of the AMOC (Trouet et al., 2009; Wanamaker et al., 2012). The strong (weak) NAO during the MCA (LIA) contributes to enhanced (weakened) AMOC through enhancing (weakening) the westerly (Trouet et al., 2009). Solar activity is usually considered as the root trigger of natural climate change. The Yongxing record is broadly similar to change in solar irradiance (Steinhilber et al., 2009; Fig. 6a). The intensifying EASM is paralleled with the greater solar activity during the MCA and the weakened EASM with the less solar activity during the LIA. The solar forcing of the EASM can be conducted through modulating the Asia-Pacific temperature contrast (Kutzbach et al., 2008), the AMOC intensity (Wang et al., 2005) and the ENSO condition (Asmerom et al., 2007; Zhao et al., 2016). However, relative importance of these forcing pathways is unknown and, most importantly, the ENSO condition remains a matter of debate during the last millennium (e.g., Cobb et al., 2003; Yan et al., 2011a). As a counterpart to the MCA, the CWP is similarly marked by intensified EASM, strong AMOC and high solar output (Fig. 6). However, the relationship between the EASM and NAO becomes unclear during the CWP, with the intensified EASM failing to match the expected more positive NAO. Longer term data is needed to assess the linkage between NAO and EASM during the CWP.

5 Conclusions

Based on a new and published stalagmite records from the Yongxing cave, central China, we reconstruct a continuous evolutional history of the EASM during the past millennium and link its variation with the Pacific and North Atlantic climates. The climatic features in our record are generally in agreement with those in the Wanxiang and Huangye cave records in northern China as well as the Dongge cave record in southern China. The agreement consolidates our EASM reconstruction by the Yongxing records. The intensified (weakened) EASM during the MCA (LIA) correlates with the warm (cold) surface temperature and enhanced (reduced) rainfall over the IPWP. Based on the strong correlation with the ENSO reconstruction, our records support an El Nino- like condition during the MCA and a La Nina-like condition during the LIA. In addition, our records show a potential link between the EASM and the North Atlantic climate. The intensified EASM coincides with positive NAO and robust AMOC during the MCA, while the weakened EASM corresponds with neutral to negative NAO and weak AMOC during the LIA.

Acknowledgments

This work was supported by Zhejiang Provincial Natural Science Foundation (no. LY19D020001) and National Natural Science Foundation of China grants (nos. 41602181, 41572340 and 41572151).

References

An, Z., Clemens, S., Shen, J., Qiang, X., Jin, Z., Sun, Y., Prell, W., Luo, J., Wang, S., Xu, H., Cai, Y., Zhou, W., Liu, W., Shi, Z., Yan, L., Xiao, X., Chang, H., Wu, F., Ai, L., and Lu, F.: Glacial-interglacial Indian summer monsoon dynamics, science, 333, 719-723, 2011.

Asmerom, Y., Polyak, V., Burns, S., and Rassmussen, J.: Solar forcing of Holocene climate: New insights from a speleothem record, southwestern United States, Geology, 35, 1-4, 2007.

Böhm, E., Lippold, J., Gutjahr, M., Frank, M., Blaser, P., Antz, B., Fohlmeister, J., Frank, N., Anderson, M. B., and Deininger, M.: Strong and deep Atlantic meridional overturning circulation during the last glacial cycle, Nature, 517, 73-76, 2015.

Bond, G., Kromer, B., Beer, J., Muscheler, R., Evans, M., Showers, W., Hoffmann, R., Lotti-Bond, R. Hajdas, I., and Bonani, G.: Persistent Solar Influence on North Atlantic Climate During the Holocene, Science, 294, 2130-2136, 2001.

Bradley, R., Hughes, M., and Diaz, H.: Climate in Medieval Time, Science, 302, 404-405, 2003.

Chen, J., Chen, F., Feng, S., Huang, W., Liu, J., and Zhou, A.: Hydroclimatic changes in China and surroundings during the Medieval Climate Anomaly and Little Ice Age: spatial patterns and possible mechanisms, Quaternary Sci. Rev., 107, 98-111, 2015.

Chen, T., Cobb, K., Roff, G., Zhao, J., Yang, H., Hu, M., and Zhao, K.: Coral-derived western Pacific tropical sea surface temperatures during the last millennium, Geophys. Res. Lett., 45, 3542-3549, 2018.

Cheng, H., Edwards, R. L., Broecker, W. S., Denton, G. H., Kong, X., Wang, Y., Zhang, R., and Wang, X.: Ice age terminations, science, 326, 248-252, 2009.

Cheng, H., Edwards, R. L., Sinha, A., Spötl, C., Yi, L., Chen, S., Kelly, M., Kathayat, G., Wang, X., Li, X., Kong, X., Wang, Y., Ning, Y., and Zhang, H.: The Asian monsoon over the past 640,000 years and ice age terminations, Nature, 534, 640-646, 2016.

Chu, G., Liu, J., Sun, Q., Lu, H., Gu, Z., Wang, W., and Liu, T.: The 'Mediaeval Warm Period' drought recorded in Lake Huguangyan, tropical South China, Holocene, 12, 511-516, 2002.

Cobb, K., Charles, C., Cheng, H., and Edwards, R.: El Nino/Southern Oscillation and tropical Pacific climate during the last millennium, Nature, 424, 271-276, 2003.

Deng, W., Liu, X., Chen, X., Wei, G., Zeng, T., Xie, L., and Zhao, J.: A comparison of the climates of the Medieval Climate Anomaly, Little Ice Age, and Current Warm Period reconstructed using coral records from the northern South China Sea, J. Geophys. Res.-Oceans., 122, 264–275, 2017.

Dorale, J., and Liu, Z.: Limitations of Hendy test criteria in judging the paleoclimate suitability of speleothems and the need for replication, J. Cave Karst Stud., 71,73-80, 2009.

Goldsmith, Y., Broecker, W., Xu, H., Polissar, P., deMenocal, P., Porat, N., Lan, J., Cheng, P., Zhou, W., and An, Z.: Northward extent of East Asian monsoon covaries with intensity on orbital and millennial timescales, P. Natl. Acad. Sci. USA., 114, 1817-1821, 2017.

Griffiths, M., Kimbrough, A, Gagan, M., Drysdale, R., Cole, J., Johnson, K., Zhao, J., Cook, B., Hellstrom, J., and Hantoro, W.: Western Pacific hydroclimate linked to global climate variability over the past two millennia, Nat. Commun., 7, 11719, 2016.

Haug, G., Hughen, K., Sigman, D., Peterson, L., and Röhl, U.: Southward migration of the intertropical convergence zone through the Holocene, Science, 293, 1304-1308, 2001.

He, B., Zhang, S., and Cai, S.: Climatic changes recorded in peat from the Dajiu Lake basin in Shennongjia since the last 2600 years, Mar. Geol. Quat. Geol., 23, 109-115, 2003 (in Chinese with English abstract).

Jiang, X., Wang, X., He, Y., Hu, H. M., Li, Z., Spötl, C., and Shen, C. C.: Precisely dated multidecadally resolved Asian summer monsoon dynamics 113.5–86.6 thousand years ago, Quaternary Sci. Rev., 143, 1-12, 2016.

Kutzbach, J., Liu, X., Liu, Z., and Chen, G.: Simulation of the evolutionary response of global summer monsoons to orbital forcing over the past 280,000 years, Clim. Dynam., 2008, 30, 567-579, 2008.

Li, T., Shen, C., Huang, J., Jiang, X., Yang, X., Mii, H., Lee, S., and Lo, L.: Stalagmite-inferred variability of the Asian summer monsoon during the penultimate glacial-interglacial period, Clim. Past., 10, 1211-1219, 2014.

Maher, B., and Thompson, R.: Oxygen isotopes from Chinese caves: records not of monsoon rainfall but of circulation regime, J. Quaternary Sci., 27, 615-624, 2012.

Mann, M., Zhang, Z., Hughes, M., Bradley, R., Miller, S., Rutherford, S., and Ni, F.: Proxy-Based Reconstructions of Hemispheric and Global Surface Temperature Variations over the Past Two Millennia, P. Natl. Acad. Sci. USA., 105, 13252-13257, 2008.

Mann, M., Zhang, Z., Rutherford, S., and Bradley, R., Hughes, M., Shindell, D., Ammann, C., Faluvegi, G., and Ni, F.: Global Signatures and Dynamical Origins of the Little Ice Age and Medieval Climate Anomaly, Science, 326, 1256-1260, 2009.

Moy, C., Seltzer, G., Rodbell, D., and Anderson. D.: Variability of El Niño/Southern Oscillation activity at millennial timescales during the Holocene epoch, Nature, 420, 162-165, 2002.

Oppo, D., Rosenthal, Y., and Linsley, B.: 2,000-year-long temperature and hydrology reconstructions from the Indo-Pacific warm pool, Nature, 460, 1113-1116, 2009.

Orland, I., Edwards, R., Cheng, H., Kozdon, R., Cross, M., and Valley, J.: Direct measurements of deglacial monsoon strength in a Chinese stalagmite, Geology, 2015, 43, 555-558, 2015.

Overpeck, J., Anderson, D., Trumbore, S., and Prell, W.: The southwest Indian Monsoon over the last 18000 years, Clim. Dynam., 12:213-225, 1996.

Owen, R., Day, C., Hu, C., Liu, Y., Pointing, M., Blättler, C., and Henderson, G.: Calcium isotopes in caves as a proxy for aridity: Modern calibration and application to the 8.2 kyr event, Earth Planet. Sci. Lett., 443, 129-138, 2016.

PAGES 2k Consortium.: Continental-scale temperature variability during the past two millennia, Nat. Geosci., 2013, 6, 339-346, 2013.

Pausata, F., Battisti D., Nisancioglu, K., and Bitz, C.: Chinese stalagmite $\delta^{18}O$ controlled by changes in the Indian monsoon during a simulated Heinrich event, Nat. Geosci., 4: 474-480, 2011.

Rustic, G., Koutavas, A., Marchitto, T., and Linsley, B.: Dynamical excitation of the tropical Pacific Ocean and ENSO variability by Little Ice Age cooling, Science, 350, 1537-1541, 2015.

Scholz, D., and Hoffmann, D.: StalAge-An algorithm designed for construction of speleothem age models, Quat. Geochronol., 6, 369-382, 2011.

Shao, Q., Pons-Branchu, E., Zhu, Q., Wang, W., Valladas, H., and Fontugne, M.: High precision U/Th dating of the rock paintings at Mt. Huashan, Guangxi, southern China, Quat. Res., 88, 1-13, 2017.

Steinhilber, F., Beer, J., and Frohlich, C.: Total solar irradiance during the Holocene, Geophys. Res. Lett., 36, L19704, https://doi.org/10.1029/2009GL040142, 2009.

Tan, L., Cai, Y., An, Z., Edwards, R., Cheng, H., Shen, C., and Zhang, H.: Centennial-to decadal-scale monsoon precipitation variability in the semi-humid region, northern China during the last 1860 years: Records from stalagmites in Huangye Cave, Holocene, 21, 287-296, 2011.

Tan, L., Cai, Y., Cheng, H., Edwards, R., Shen, C., Gao, Y., and An, Z.: Climate significance of speleothem $\delta^{18}O$ from central China on decadal timescale, J. Asian Earth Sci., 106, 150-155, 2015.

Tan, L., Cai, Y., Cheng, H., An, Z., and Edwards, R.: Summer monsoon precipitation variations in central China over the past 750 years derived from a high-resolution absolute-dated stalagmite, Palaeogeogr. Palaeocl., 280, 432-439, 2009.

Tan, L., Cai, Y., Cheng, H., Edwards, L., Lan J., Zhang, H., Li, D., Ma, L., Zhao, P., and Gao, Y.: High resolution monsoon precipitation changes on southeastern Tibetan Plateau over the past 2300 years, Quaternary Sci. Rev., 195, 122-132, 2018.

Tan, M., Liu, D., Hou, J., Qin, X., Zhang, H., and Li, T.: Cyclic rapid warming on centennial-scale revealed by a 2650-year stalagmite record of warm season temperature, Geophys. Res. Lett., 30, 1617, https://doi.org/10.1029/2003GL017352, 2003.

Tan, M.: Circulation effect: response of precipitation $\delta^{18}O$ to the ENSO cycle in monsoon regions of China, Clim. Dyn., 42, 1067-1077, 2014.

Thornalley, D., Oppo, D., Ortega, P., Robson, J., Brierley, C., Davis, R., Hall, I., Moffa-Sanchez, P., Rose, N., Spooner, P., Yashayaev, I., and Keigwin, L.: Anomalously weak Labrador Sea convection and Atlantic overturning during the past 150 years, Nature, 556, 227-230, 2018.

Trouet, V., Esper, J., Graham, N., Baker, A., Scourse, J., and Frank, D.: Persistent Positive North Atlantic Oscillation Mode Dominated the Medieval Climate Anomaly, Science, 324, 78-80, 2009.

Wanamaker Jr, A., Butler, P., Scourse, J., Heinemeier, J., Eiríksson, J., Knudsen, K., and Richardson, C.: Surface changes in the North Atlantic meridional overturning circulation during the last millennium, Nat. Commun., 3, 899, 2012.

Wang, B., Liu, J., Kim, H., Webster, P., Yim, S. and Xiang, B.: Northern Hemisphere summer monsoon intensified by mega-El Nino/southern oscillation and Atlantic multidecadal oscillation, P. Natl. Acad. Sci. USA., 110, 5347-5352, 2013.

Wang, Q., Wang, Y., Zhao, K., Chen, S., Liu, D., Zhang, Z., Huang, W., Yang, S., and Liang, Y.: The transfer of oxygen isotopic signals from precipitation to drip water and modern calcite on the seasonal time scale in Yongxing Cave, central China, Environ. Earth Sci., 77, 474, 2018.

Wang, X., Edwards, R., Auler, A., Cheng, H., Kong, X., Wang, Y., Cruz, F., Dorale, J., and Chiang, H.: Hydroclimate changes across the Amazon lowlands over the past 45,000 years, Nature, 541, 204-207, 2017.

Wang, Y., Wang, B., Oh, J.: Impact of the preceding El Niño on the East Asian summer

atmosphere circulation, J. Meteorol. Soc. Jpn., 79, 575-588, 2001.
Wang, Y., Cheng, H., Edwards, R., An, Z., Wu, J., Shen, C., and Dorale, J.: A high-resolution absolute-dated late Pleistocene monsoon record from Hulu Cave, China, Science, 294, 2345–2348, 2001.
Wang, Y., Cheng, H., Edwards, R., He, Y., Kong, X., An, Z., Wu, J., Kelly, M., Dykoski, C., and Li, X.: The Holocene Asian mon-soon: Links to solar changes and North Atlantic climate, Science, 308, 854–857, 2005.
Xu, H., Lan, J., Sheng, E., Liu, B., Yu, K., Ye, Y., Shi, Z., Cheng, P., Wang, X., Zhou, X., and Yeager, K.: Hydroclimatic contrasts over Asian monsoon areas and linkages to tropical Pacific SSTs, Sci. Rep., 6, 33177, 2016.
Yan, H., Sun, L., Oppo, D., Wang, Y., Liu, Z., Xie, Z., Liu, X., and Cheng, W.: South China Sea hydrological changes and Pacific Walker Circulation variations over the last millennium, Nat. Commun., 2, 293, 2011a.
Yan, H., Sun, L., Wang, Y., Huang, W., Qiu, S., and Yang, C.: A record of the Southern Oscillation Index for the past 2,000 years from precipitation proxies, Nat. Geosci., 4, 611-614, 2011b.
Yan, H., Wei, W., Soon, W., An, Z., Zhou, W., Liu, Z., Wang, Y., and Carter, R.: Dynamics of the intertropical convergence zone over the western Pacific during the Little Ice Age, Nat. Geosci., 8, 315, 2015.
Yuan, D., Cheng, H., Edwards, R., Dykoski, C., Kelly, M., Zhang, M., Qing, J., Lin, Y., Wang, Y., Wu, J., Dorale, J., An, Z., and Cai, Y.: Timing, durationand transitions of the last interglacial Asian monsoon, Science, 304, 575-578, 2004.
Zhang, P., Cheng, H., Edwards, R., Chen, F., Wang, Y., Yang, X., Liu, J., Tan, M., Wang, X., Liu, J., An, C., Dai, Z., Zhou, J., Zhang, D., Jia, J., Jin, L., and Johnson, K.: A test of climate, sun, and culture relationships from an 1810-year Chinese cave record, Science, 322, 940-942, 2008.
Zhang, W., Chen, S., Wang, Y., Zhao, K., Shao, Q., Wang, T., and Zhu, L.: Rapid changes in the East Asian summer monsoon: stalagmite records in Hubei, China, Quaternary Sci., 39, 765-774, 2019 (in Chinese with English abstract).
Zhao, K., Wang, Y., Edwards, R., Cheng, H., Liu, D., and Kong, X.: A high-resolved record of the Asian Summer Monsoon from Dongge Cave, China for the past 1200 years, Quaternary Sci. Rev., 122, 250-257, 2015.
Zhao, K., Wang, Y., Edwards, R., Cheng, H., Liu, D., Kong, X., and Ning, Y.: Contribution of ENSO variability to the East Asian summer monsoon in the late Holocene, Palaeogeogr. Palaeocl., 449, 510-519, 2016.
Zhao, K., Wang, Y., Edwards, R., Cheng, H., and Liu, D.: High-resolution stalagmite $\delta^{18}O$ records of Asian monsoon changes in central and southern China spanning the MIS3/2 transition, Earth Planet Sci. Lett., 298, 191–198, 2010.

Table and figure

Table l U-series dating results of stalagmite YX262 from Yongxing Cave

Sample depth (mm)	^{238}U (ppb)	^{232}Th (ppt)	δ^{234}U (measured)	^{230}Th/^{238}U (activity)	^{230}Th Age (a) (uncorrected)	δ^{234}U$_{initial}$ (corrected)	^{230}Th Age (a) (corrected)
YX262-5	546.0 ±0.5	307.9 ±0.6	607.5 ±1.0	0.006230157 ±0.00014	423.5 ±9.4	608.2 ±1.0	413.1 ±10.8
YX262-25	595.5 ±03	280.5 ±0.6	790.6 ±1.9	0.00788248 ±0.00008	481.0 ±5.1	791.7 ±1.9	473.1 ±6.3
YX262-48	506.3 ±03	281.6 ±0.5	762.1 ±1.9	0.009468079 ±0.00010	587.3 ±6.4	763.4 ±1.9	577.9 ±8.0
YX262-75	517.7 ±03	724.3 ±0.1	680.5 ±2.1	0.010930422 ±0.00010	711.3 ±6.4	681.8 ±2.1	686.3 ±13.9
YX262-95	651.8 ±03	1448.0 ±0.3	806.5 ±2.0	0.013146471 ±0.00010	796.0 ±6.3	808.3 ±2.0	759.4 ±19.1
YX262-116	583.4 ±08	283.0 ±0.4	956.6 ±1.0	0.014987259 ±0.00012	838.0 ±6.6	958.9 ±1.0	830.8 ±7.5

Decay constant values are λ_{234}=2.82206×10^{-6}a^{-1}, λ_{238}=1.55125×10^{-10}a^{-1}, λ_{230}=9.1705×10^{-16}a^{-1} and δ^{234}U = ([^{234}U/^{238}U]$_{activity}$-1)×1000. Corrected ^{230}Th age calculation, indicated in bold, is based on an assumed initial ^{230}Th/^{232}Th atomic ratio of (4 ±2) ×10^{-6}. All corrected dates are years before 2017 A.D.

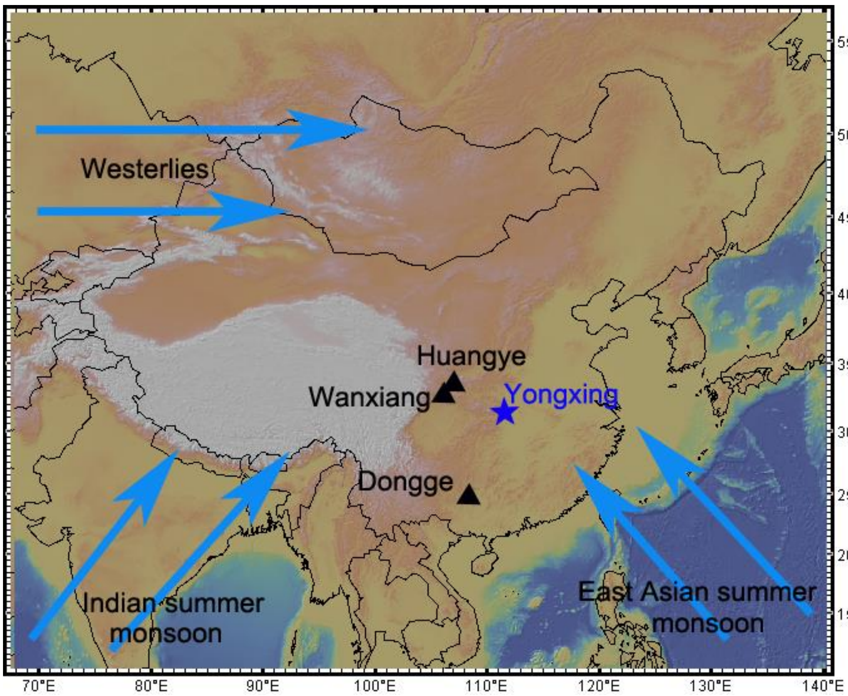

Fig.1 Schematic climate setup of East Asian Monsoon and our study site. The blue star and black triangles represent Yongxing Cave in central China and other caves in the monsoonal region, respectively.

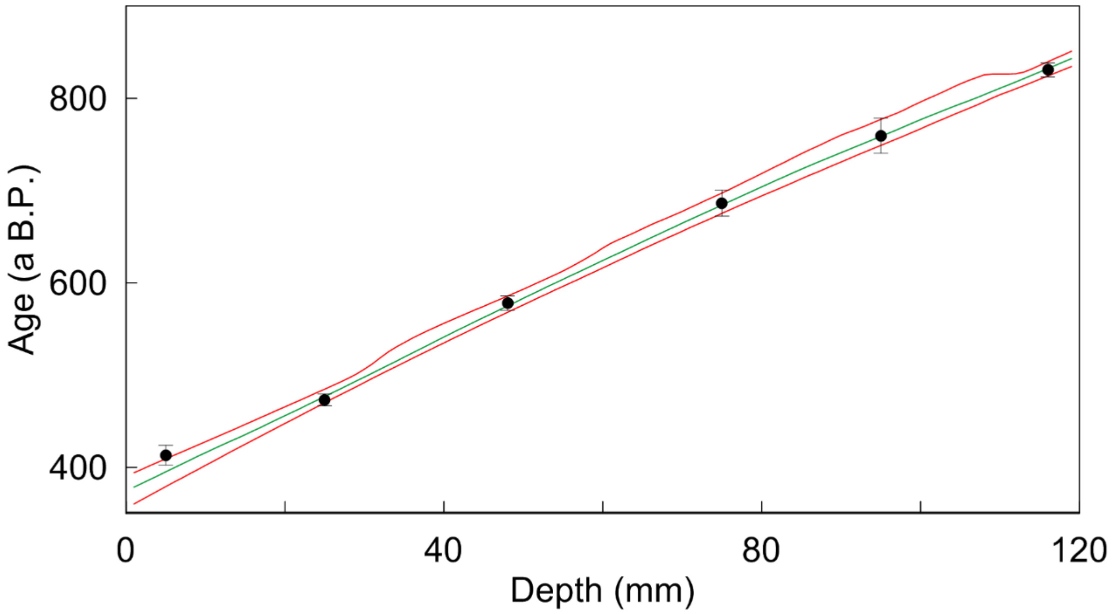

Fig. 2 Age versus depth model for our stalagmite YX262. The black dots and vertical error bars indicate ^{230}Th dates and errors of these dates, respectively. The middle green line indicates the model age, and upper and lower red lines indicate the age in 95% confidence level, respectively.

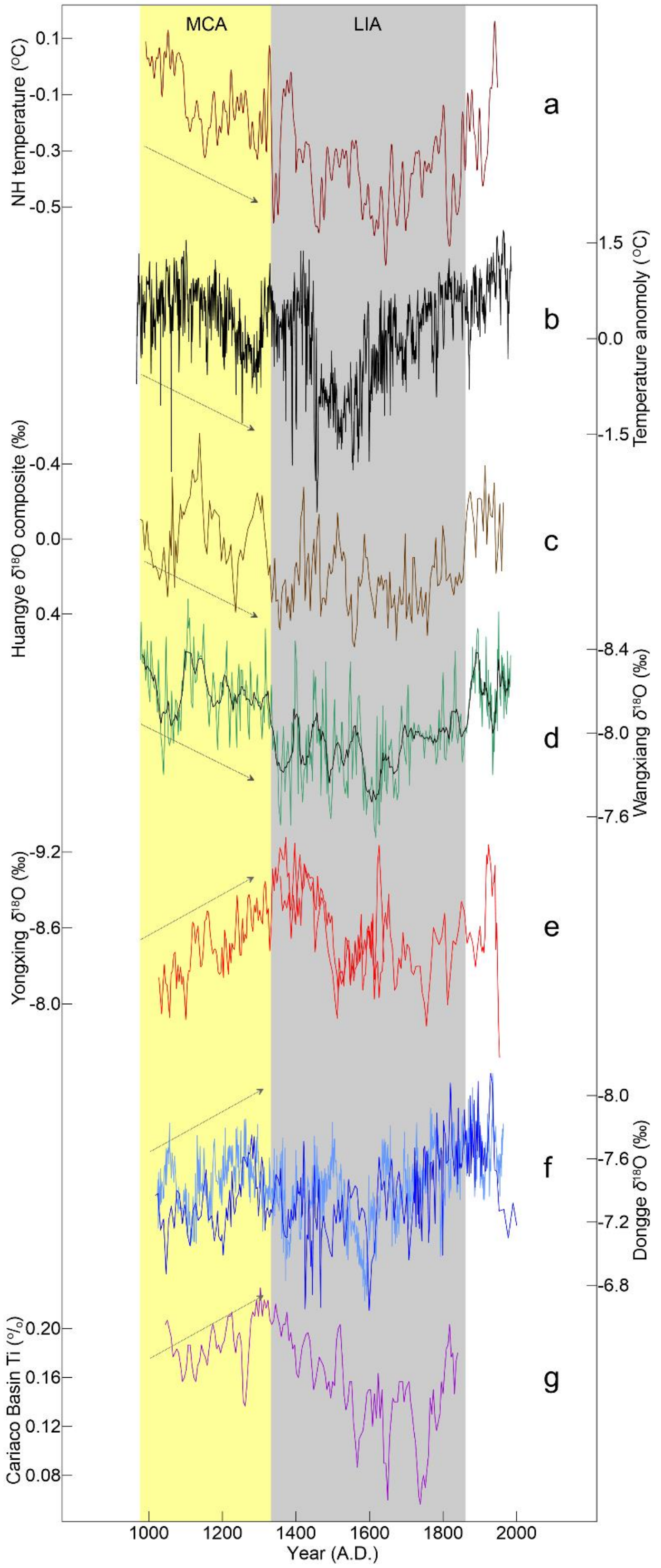

Fig. 3 A comparison of the Yongxing $\delta^{18}O$ time-series with other proxy records. (a) Northern Hemisphere reconstructed temperature (Mann et al., 2009); (b) Northern China reconstructed temperature (Tan et al., 2003); (c) Huangye Cave $\delta^{18}O$ composite (Tan et al., 2011); (d) Wanxiang Cave $\delta^{18}O$ record (Zhang et al., 2008); (e) Yongxing

Cave record (this study); (f) Dongge Cave record (Wang et al., 2005; Zhao et al., 2015); (g) Cariaco Basin Ti content record (Haug et al., 2001). Light yellow and blue bars indicate the MCA and LIA, respectively. Arrows indicate trends of the climatic variations.

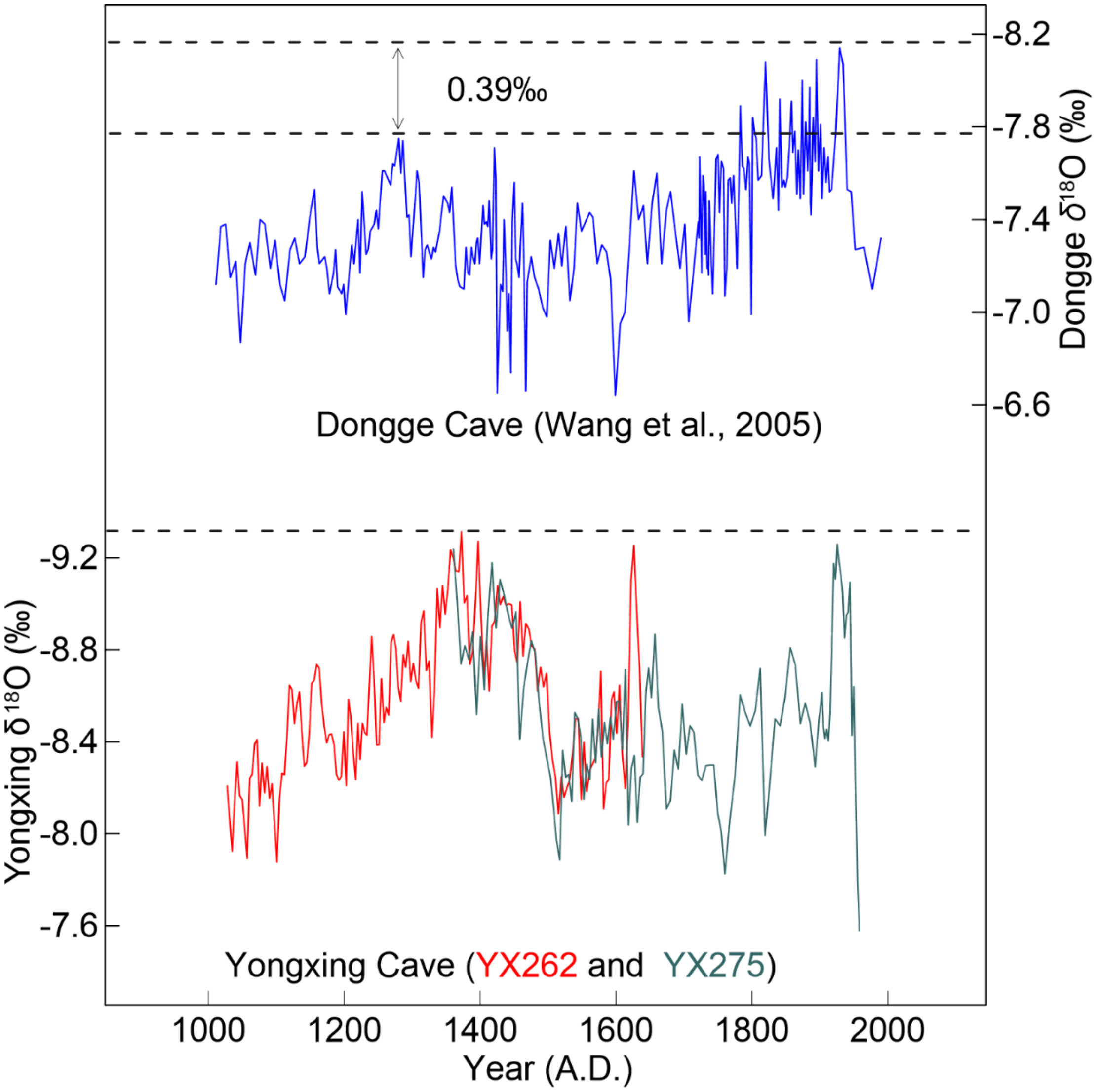

Fig. 4 Relative intensity of EASM during the MCA as compared to the CWP. The upper panel is the Dongge cave record (Wang et al., 2005); the lower panel is the Yongxing Cave YX262 (red) and YX275 (green, Zhang et al., 2019) records. On average, the Dongge Cave record shows a 0.39‰ lower $\delta^{18}O$ values during the CWP than the MCA. However, the Yongxing record shows a comparable value between the CWP and MCA.

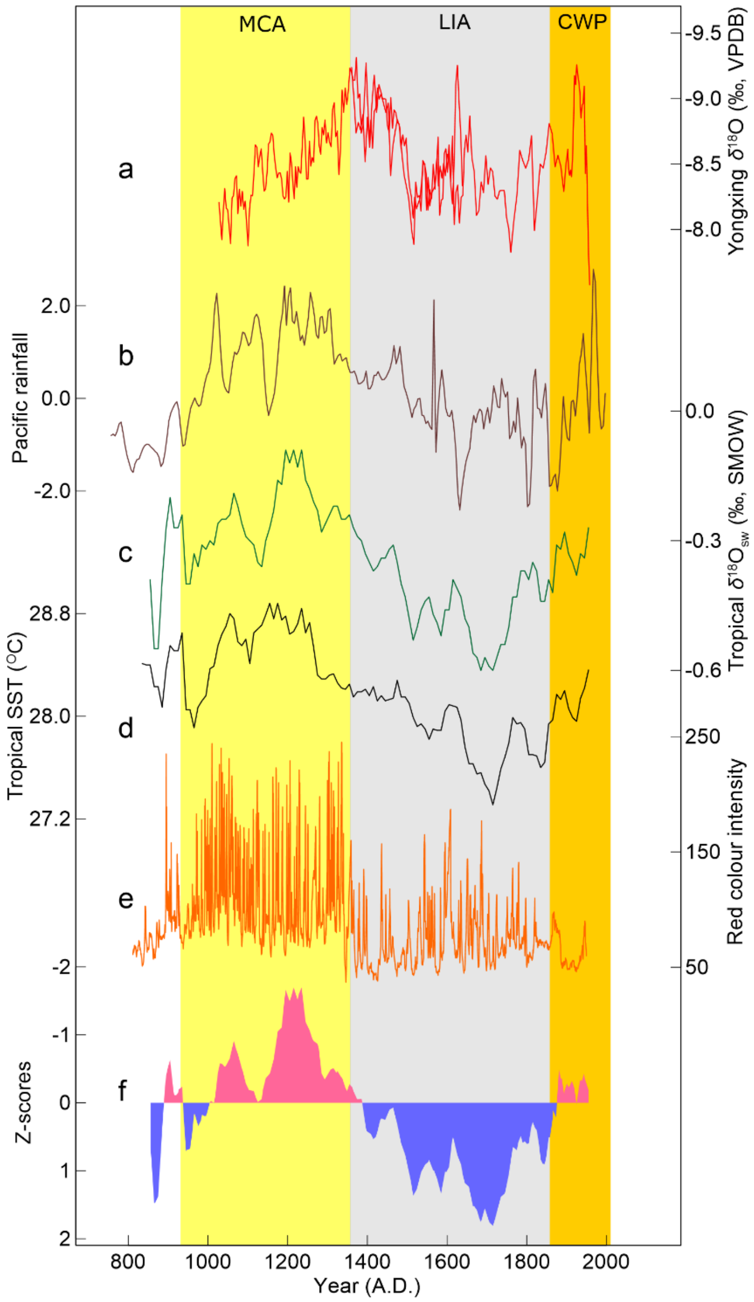

Fig. 5 A comparison between EASM and Pacific climate. (a) Yongxing cave record (this study); (b)Tropical Pacific rainfall record (Oppo et al., 2009); (c) Tropical Pacific $\delta^{18}O$ record (Oppo et al., 2009); (d) Tropical Pacific sea surface temperature (Oppo et al., 2009); (e) Red colour intensity in southern Ecuador (Moy et al., 2002); (f) Hydrological reconstruction of ENSO from Tropical Pacific (Yan et al., 2011a). Yellow, grey and orange bands represent the MCA, LIA, and CWP, respectively.

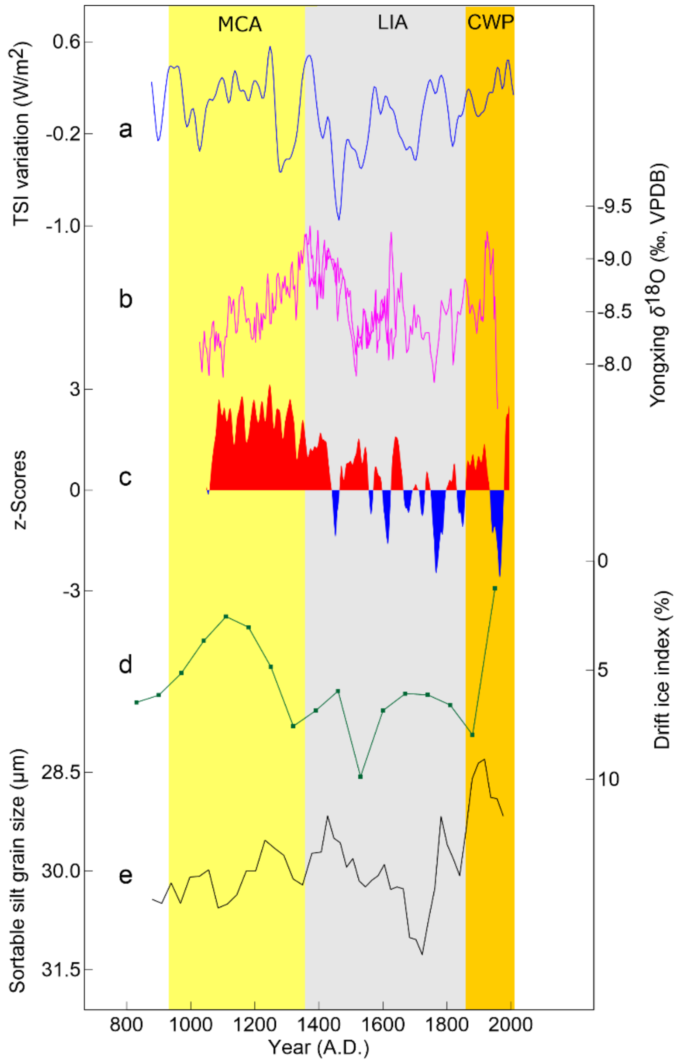

Fig. 6 A comparison between EASM, solar activity and North Atlantic climate. (a) Total solar irradiance (Steinhilber et al., 2009); (b) Yongxing Cave record (this study); (c) North Atlantic Oscillation (Trouet et al., 2009); (d) North Atlantic drift ice index (Bond et al., 2001); (e) Sortable silt grain size in the North Atlantic (Thornalley et al., 2018). Yellow, grey and orange bands represent the MCA, LIA, and CWP, respectively.